ADVANCED ENERGY & SUSTAINABILITY RESEARCH
Open Access
www.advenergysustres.com

Homogeneous Polymer Films for Passive Daytime Cooling: Optimized Thickness for Maximized Cooling Performance

Kai Herrmann, Tobias Lauster, Qimeng Song, and Markus Retsch**

Passive radiative cooling materials that spontaneously cool below ambient temperature can save tremendous amounts of energy used for cooling applications. A multitude of materials, structures, and fabrication strategies have been reported in recent years. Important material parameters like a tailored or broadband emissivity, angle selectivity, or the influence of nonradiative heat losses were discussed in detail. The material thickness has been far less researched and is typically chosen sufficiently thick to ensure high emission in the atmospheric transparency window between wavelengths of 8–13 μm. However, not only the material emittance but also atmospheric and solar energy uptake depend on the material thickness. This broadband interplay has been less addressed so far. Herein, it is shown how an optimum thickness of a passive cooling material can be predicted when the optical properties of the material are known. Using complex refractive index data, the thickness-dependent cooling performance of polydimethylsiloxane (PDMS) in back-reflector geometry as exemplary material is calculated. For both day- and nighttime operation, an optimum emitter thickness is reported. The findings are verified experimentally by measuring the equilibrium temperatures of PDMS films with different thicknesses in a rooftop experiment. The presented analytical approach is directly transferable to other materials.

1. Introduction

The field of passive daytime radiative cooling materials has significantly developed in the last decade. Many new materials emerged that show a cooling effect below ambient temperature, even with direct sunlight illumination.[1] The key to achieving a net cooling power is minimizing energy absorption and maximizing energy emission. A multitude of approaches were proposed that lead to the desired optical properties, including photonic structures,[2] polymeric materials,[3] and composite materials.[4]

A material is primarily a good candidate for passive radiative cooling if it exhibits a high emissivity in the wavelength range of thermal radiation at ambient temperature. This wavelength range is located in the mid to far infrared (IR) region (≈3–50 μm). Second, a low absorptivity in the solar region is required because any energy uptake from the sun directly reduces the cooling power. This energy absorption is prevented by including a reflective metal layer below the emitter material,[4b,5] using a solar filter approach,[6] or by efficient scattering of solar wavelengths by the material itself.[3a,7] Third and most complex is to avoid radiative energy uptake by the surrounding atmosphere. As this radiance appears in a similar wavelength regime as the emitted thermal radiation, special care must be taken. The most common approach here is to focus emission on the first (8–13 μm) and second (16–28 μm) atmospheric transmission window where low atmospheric radiation is present. With a confined emission in this spectral region, the lowest temperatures below ambient can be reached. However, the cooling power at ambient temperature is reduced in comparison to a blackbody emitter.[1a,8]

The material thickness is an essential parameter for the applicability of passive cooling materials and was discussed by several groups in the literature.[5b,9] For example, in the work of Zhou et al., a PDMS layer on an aluminum substrate is considered.[5b] The authors chose a 150 μm-thick layer and found that above 100 μm thickness, the emissivity in the 8–13 μm wavelength range was close to unity. In the work of Zhu et al., the thickness of a PDMS layer on a reflective silver layer was discussed, and a thickness of 200 μm was suggested.[9b] The authors found that up to this thickness, the emissivity in the wavelength range from 2.5 to 25 μm was increasing, but for a higher thickness of 300 μm, there were only minor changes. Besides PDMS as emitting layer, the group of Zhu et al. investigated the thickness of a composite material consisting of In_2O_3 particles in a polymethyl methacrylate matrix.[10] They found the thickness of their composite needs to be larger than 25 μm to have high emissivity within the

K. Herrmann, T. Lauster, Q. Song, M. Retsch
Department of Chemistry, Physical Chemistry I
University of Bayreuth
Universitätsstraße 30, 95447 Bayreuth, Germany
E-mail: qimeng.song@uni-bayreuth.de; markus.retsch@uni-bayreuth.de
M. Retsch
Bavarian Polymer Institute
Bayreuth Center for Colloids and Interfaces
and Bavarian Center for Battery Technology (BayBatt)
University of Bayreuth
Universitätsstraße 30, 95447 Bayreuth, Germany
The ORCID identification number(s) for the author(s) of this article can be found under https://doi.org/10.1002/aesr.202100166.

DOI: 10.1002/aesr.202100166

first and second atmospheric window. In the work of Tian et al., poly-4-methyl-1-pentene (PMP) films of different thicknesses are used to determine the complex refractive index of the material.[9a] In this work, the investigated film with a thickness of 1283 µm was found to have the highest absorptance within the first and second atmospheric window. In all this previous work, the emitter thickness was optimized to maximize the emission within the first and/or second atmospheric window. However, the material thickness also affects the solar absorption and atmospheric energy uptake behavior of a material simultaneously. This interplay of thickness dependencies for the different energetic contributions has been barely addressed so far. The relevance of optical thickness in the solar range becomes even more relevant, considering emerging aesthetic passive cooling designs, where colored films are fabricated. As long as coloration is not based on Bragg diffraction,[11] a suitable tradeoff between color impression and thermal load based on the absorption and thermalization process[12] needs to be found.

This work focuses on PDMS as an often used and well-characterized passive cooling material to conceptually address the optimum thickness of an emitter material. Our study provides a theoretical approach based only on the fundamental optical constants for estimating the optimum emitter thickness. Experimental data subsequently verify the outlined theoretical framework. Therefore, PDMS thin films of several thicknesses on Ag mirrors were prepared to determine the equilibrium temperatures below ambient during day- and nighttime. In conclusion, we point out how to optimize the sample thickness of a given emitter material for passive day- and nighttime cooling applications in the back-reflector geometry.

2. Theoretical Approach

To determine the optimum thickness, we first derive how the individual energetic contributions of a passive cooling material depend on the emitter material thickness. Taking into account all the energy exchange processes, the net cooling power P_{cool} can be defined as[1a]

$$P_{\text{cool}} = P_{\text{mat}} - P_{\text{sun}} - P_{\text{atm}} - P_{\text{nonrad}} \tag{1}$$

where P_{mat} represents the energy radiated by the material, P_{sun} the absorbed energy due to solar radiation, P_{atm} the absorbed energy due to atmospheric radiation, and P_{nonrad} intrinsic losses due to convection and conduction. The considered energy exchange processes are schematically shown in **Figure 1**.

To calculate the different energetic contributions, the broadband optical constants of the emitter material, a solar radiation spectrum, an atmospheric transmission spectrum, and the nonradiative heat transfer coefficient are required. Typically, the AM1.5 spectrum is used to model solar radiation. An atmospheric transmission spectrum at the measuring location is modeled using Modtran to allow for the highest accuracy possible.[13] The data used for the calculations performed in this article and a schematic for calculating the thickness-dependent angular and spectral emissivity are shown in **Figure 2**.

The energy radiated by the emitter material can be calculated using the spectral radiance I_{b} described by Planck's law, which depends on the emitter material temperature T_{mat} and the

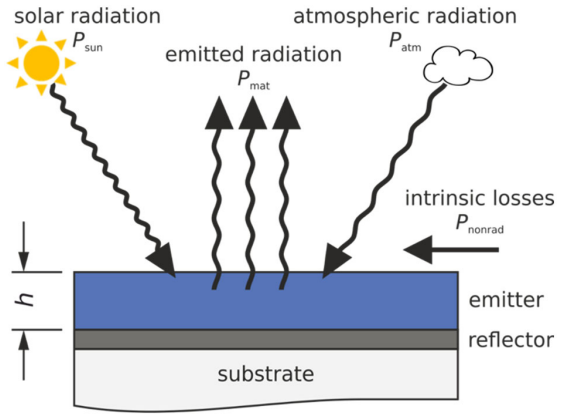

Figure 1. Schematics of the radiative cooler containing the considered energy exchange processes.

emissivity of the emitter material $\varepsilon_{\text{mat}}(\lambda, h, \theta)$, depending on wavelength λ, thickness h and polar angle θ, and the azimuthal angle φ.[1b]

$$P_{\text{mat}} = \int_0^{2\pi} d\varphi \int_0^{\pi/2} \sin\theta \cos\theta d\theta \int_0^{\infty} I_{\text{b}}(\lambda, T_{\text{mat}}) \cdot \varepsilon_{\text{mat}}(\lambda, h, \theta) d\lambda \tag{2}$$

Azimuthal dependency is not considered in our spectral-dependent and directional-dependent viewpoint and therefore reduces to a factor of 2π.

$$P_{\text{mat}} = 2\pi \int_0^{\pi/2} \sin\theta \cos\theta \int_0^{\infty} I_{\text{b}}(\lambda, T_{\text{mat}}) \cdot \varepsilon_{\text{mat}}(\lambda, h, \theta) d\lambda d\theta \tag{3}$$

Here, the thickness dependency becomes evident because the emittance of the film depends on the material thickness h. The angular and spectral emittance of the film $\varepsilon_{\text{mat}}(\lambda, h, \theta)$ is defined as $1 - R(\lambda, h, \theta)$, where $R(\lambda, h, \theta) = \frac{|E_0|^2}{|E_1|^2}$ is the reflectance, as proposed by Zhu et al.[10] A schematic representation for calculating the angular and spectral emittance is shown in Figure 2b.

To calculate the emittance, the following parameters are introduced with the Fresnel equation for s- and p-polarized waves, respectively

$$r^{\text{s}}_{\text{air,mat}} = \frac{n_{\text{air}} \cos\theta_i - n_{\text{mat}} \cos\theta_t}{n_{\text{air}} \cos\theta_i + n_{\text{mat}} \cos\theta_t} \tag{4}$$

$$r^{\text{p}}_{\text{air,mat}} = \frac{n_{\text{mat}} \cos\theta_i - n_{\text{air}} \cos\theta_t}{n_{\text{mat}} \cos\theta_i + n_{\text{air}} \cos\theta_t} \tag{5}$$

$$\cos\theta_t = \sqrt{1 - \left(\frac{n_{\text{air}}}{n_{\text{mat}}}\right)^2 \sin^2\theta_i} \tag{6}$$

Perfect reflection at the material–silver interface results in

$$\frac{|E_3|^2}{|E_2|^2} = \exp(-2\alpha \cdot h_{\text{eff}}) \tag{7}$$

With the absorption coefficient α and the angle-dependent effective thickness h_{eff} as

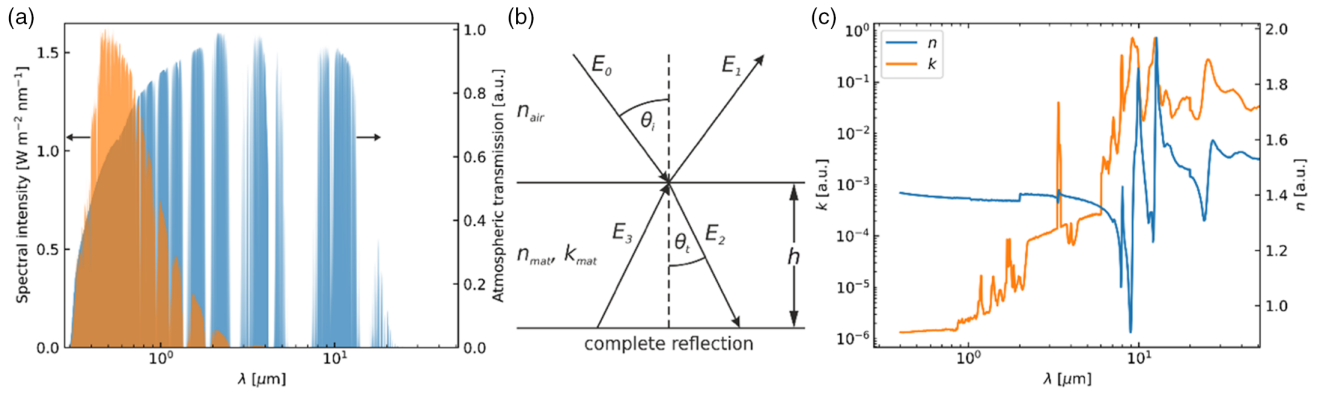

Figure 2. a) Atmospheric transmittance spectrum generated using Modtran for the measurement location (Bayreuth), as well as the employed AM1.5 solar spectrum.[13a] b) Schematics for calculating the angular and spectral emittance based on the complex refractive index of the material and its thickness. c) Utilized complex refractive index data for PDMS.[16]

$$\alpha = \frac{4\pi \cdot k}{\lambda}, \quad h_{\text{eff}} = h/\cos\theta_{\text{t}} \tag{8}$$

For an incoherent wave, one can calculate the reflectance for s- and p-polarization following the derivation of Zhu et al.[10] as

$$R^{\text{s,p}} = |r^{\text{s,p}}_{\text{air,mat}}|^2 + \frac{|1-(r^{\text{s,p}}_{\text{air,mat}})^2|^2 \exp(-2\alpha \cdot h_{\text{eff}})}{1-|r^{\text{s,p}}_{\text{air,mat}}|^2 \exp(-2\alpha \cdot h_{\text{eff}})} \tag{9}$$

The spectral-, thickness-, and angular-dependent emittance is then finally calculated as

$$\varepsilon_{\text{mat}}(\lambda, h, \theta) = 1 - \frac{R^{\text{s}} + R^{\text{p}}}{2} \tag{10}$$

The thickness dependency of the material's emittance is apparent in the energy radiated by the material and the energies absorbed due to solar and atmospheric radiation. As for the incoming radiation from the sun, a fixed position is used with $\theta_{\text{sun}} = 48.2°$ for AM1.5 conditions, the angular integration vanishes, and only a spectral integration is performed.

$$P_{\text{sun}} = \int_0^\infty I_{\text{AM1.5}}(\lambda) \cdot \varepsilon_{\text{mat}}(\lambda, h, \theta_{\text{sun}}) \text{d}\lambda \tag{11}$$

Here, $I_{\text{AM1.5}}$ denotes the AM1.5 spectral distribution of solar radiation depicted in Figure 2a. In contrast, for incoming radiation from the atmosphere, the angular integration has to be performed.

$$P_{\text{atm}} = 2\pi \int_0^{\pi/2} \sin\theta \cos\theta \int_0^\infty I_b(\lambda, T_{\text{atm}}) \cdot \varepsilon_{\text{atm}}(\lambda, \theta) \cdot \varepsilon_{\text{mat}}(\lambda, h, \theta) \text{d}\lambda \text{d}\theta \tag{12}$$

where $\varepsilon_{\text{atm}}(\lambda, \theta) = 1 - \tau_{\text{atm}}(\lambda, 0)^{1/\cos\theta}$ with $\tau_{\text{atm}}(\lambda, 0)$ being the spectral transmittance of the atmosphere at zero zenith angle depicted in Figure 2a.[14] Intrinsic losses due to convection and conduction are treated with a comprehensive heat transfer coefficient h_{nonrad}.

$$P_{\text{nonrad}} = h_{\text{nonrad}} \cdot (T_{\text{atm}} - T_{\text{mat}}) \tag{13}$$

This heat transfer coefficient is taken as an average of literature values with $h_{\text{nonrad}} = 4.4\,\text{W m}^{-2}\text{K}^{-1}$.[1b,2a,10,14,15] Instead of performing the spectral integration from zero to infinity, the upper boundary is set to 55 μm due to limited data availability. This limit is justified because approximately 97% of the emitted thermal energy at 298 K is confined to wavelengths below 55 μm. Furthermore, convergence of the resulting cooling power as a function of the upper integration boundary is shown in Figure S1, Supporting Information. Moreover, the influence of the comprehensive heat transfer coefficient h_{nonrad} is also shown in Figure S2, Supporting Information.

3. Results and Discussion

3.1. Calculations

To illustrate the concept of an optimum emitter thickness, we first examine the individual energetic contributions for PDMS at T_{amb}. At ambient temperature, the nonradiative contributions P_{nonrad} can be discarded, as no intrinsic losses due to conduction or convection are present, and emitter and atmospheric thermal radiation are modeled at the same temperature. The remaining contributions of Equation (1) and the resulting cooling power at ambient temperature are depicted in **Figure 3**.

Figure 3a displays the daytime case, revealing an optimum emitter thickness where the resulting cooling power is maximized. At low thicknesses P_{mat} and P_{atm} exhibit an increase. This is the case because the absorption coefficient of PDMS has the highest order of magnitude in the IR regime where P_{mat} and P_{atm} have their origin. At thicknesses above 1×10^{-4} m, those contributions reach a quasiplateau, where the difference between them remains approximately constant. At the same time, for emitter thicknesses above 1×10^{-5} m, the absorption in the solar wavelength regime is no longer negligible. The absorbed energy due to solar radiation increases, with further increasing the emitter thickness. The counterbalance between the increasing emitted power below 1×10^{-4} m and the

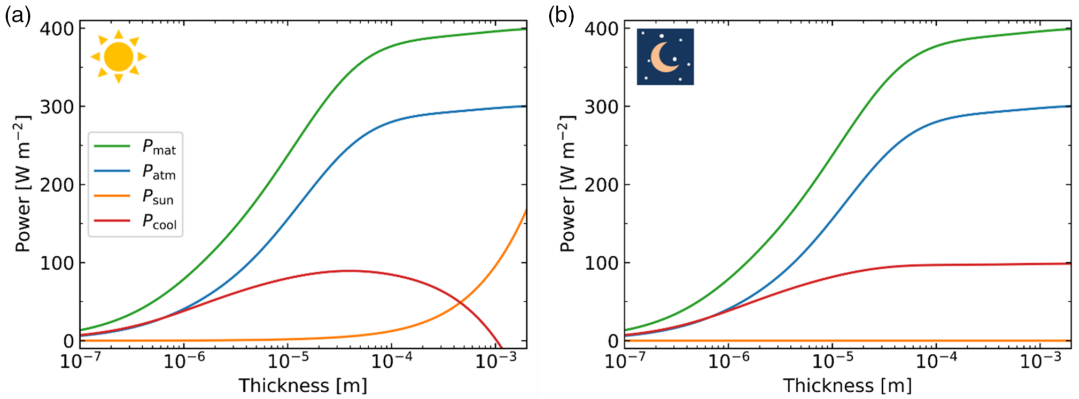

Figure 3. Individual energetic components contributing at ambient temperature as a function of thickness, as well as the resulting cooling power, during a) daytime and b) nighttime.

increasing absorbed power due to solar radiation above 1×10^{-5} m, therefore, leads to a maximum cooling power as a function of emitter thickness. For the nighttime case in Figure 3b, the contribution of solar radiation is zero, leading to a plateau being reached at high emitter thicknesses. Even as the emitted power and the power absorbed due to atmospheric radiation both continue to increase with increasing emitter thickness, the resulting cooling power asymptotically approaches a constant value. Therefore, no optimum thickness is apparent, but a minimum thickness required to reach the highest cooling power can be estimated.

After the individual contributions have been treated as a function of thickness at ambient temperature, the resulting cooling power for PDMS as a function of emitter thickness and emitter temperature is shown in **Figure 4**. Here, the cooling power is color-coded and displayed as a function of thickness and temperature difference relative to the atmospheric temperature. Negative cooling powers, equivalent to a sample that heats up, are not shown for simplicity. The boundary of the color-coded area thus represents the achievable equilibrium temperatures below ambient for the respective thickness. Red dots highlight the thickness with the highest cooling power at the respective temperature below ambient.

In general, the cooling power decreases as the material cools below ambient temperature ($T_{atm} - T_{mat} > 0$), as the blackbody radiation is reduced, and nonradiative heat transfer is apparent. An optimum thickness effect can be recognized in both the maximum cooling power at ambient, as discussed above, and the minimum equilibrium temperature below ambient, and therefore the highest temperature difference, for the daytime case. A slight shift of the highest cooling power to lower thicknesses with increasing the temperature difference between material and ambient is apparent. This shift can be understood as the emitted power approximately scales with temperature to the fourth power. A lower emitted power due to a lower emitter temperature is then counterbalanced by the incoming solar and atmospheric radiation at lower thicknesses. Our result confirms that a cooler with a certain thickness can either reach the lowest possible equilibrium temperature or the highest cooling power at ambient temperature. Conceptually, both cannot be optimized simultaneously, even as the absolute thickness values only differ by half an order of magnitude. This distinction was also the subject of discussion by other researchers when comparing different artificial emitter materials, where a blackbody emitter has higher cooling power at ambient but selective emitters can reach lower equilibrium temperatures.[1a,8]

The resulting cooling power as a function of thickness and temperature during nighttime for PDMS is shown in Figure 4b. Close to ambient, as discussed in Figure 3b, the cooling power asymptotically approaches a maximum value, where

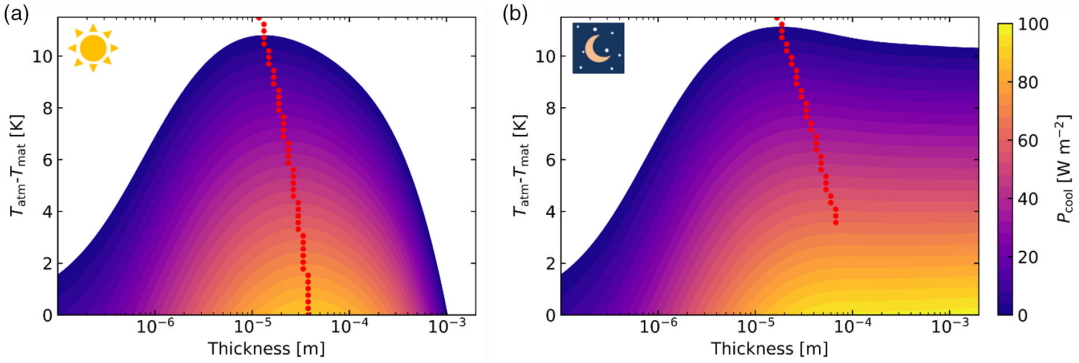

Figure 4. Resulting cooling power as a function of thickness and emitter temperature, as well as highlighted thickness (red dots) with the highest cooling power at the respective temperature, during a) daytime and b) nighttime.

an increase in thickness only incrementally increases the maximum cooling power due to the exponential nature of the material emissivity. Compared to the daytime case, higher cooling powers and lower equilibrium temperatures can be reached due to the absence of solar radiation. Only above a certain temperature difference threshold, an optimum thickness in a similar order of magnitude as for the daytime case becomes apparent. This effect is discussed in Figure S3, Supporting Information, as the effect is significantly less pronounced than during daytime. In general, for materials with different optical properties, an optimum thickness for the nighttime cooling power may be more strongly pronounced and should, therefore, be separately verified.

The main difference between day- and nighttime is a clearly defined optimum emitter thickness during daytime. In contrast, a plateau is reached at high emitter thicknesses during nighttime, and only above a certain temperature difference threshold, an optimum thickness becomes apparent.

To point out that this is a general effect and not only applicable to PDMS, we performed similar calculations for other commercial polymeric materials, i.e., polystyrene (PS), polymethyl methacrylate (PMMA), and polyethylene terephthalate (PET), where broadband complex refractive index data are available in the literature.[16a] There, the same basic principles of optimum emitter thickness apply and are shown in Figure S4, Supporting Information.

3.2. Sample Characterization

To confirm our theoretical observations, we prepared a set of PDMS films with different thicknesses and characterized their absorption properties with UV–vis and FTIR spectroscopy. Further, we conducted rooftop experiments to determine the reached equilibrium temperatures (see Experimental Section).

The actual absorptance of PDMS films with different thicknesses on reflecting Ag films is displayed in **Figure 5**. For thinner PDMS layers, the emission is more confined within the first atmospheric window. We attribute this to the high absorption coefficient of the material in this spectral region. For higher thicknesses, the absorptance in the near-IR region is substantially increasing, leading to an overall increase in emitted radiation. However, at the same time, the absorption of solar radiation is promoted. The silver mirror efficiently reflects all wavelengths larger than 400 nm and, therefore, prevents absorption of solar radiation by the underlying substrate. However, for shorter wavelengths, the absorptance increases. This loss in cooling power cannot be avoided in our sample geometry and leads to reduced cooling power in the daytime case.

To compare if the used optical data can adequately describe our samples, we calculated the absorptance for the respective thicknesses based on the complex refractive index. The resulting absorptance spectra (Figure S5, Supporting Information) capture the main features in the mid-IR region. However, in the solar region, larger deviations for the thickest sample are evident. Therefore, the exact determination of the complex refractive index is crucial for a prediction of the cooling performance. Substantial variations in the absorption coefficient can be expected for every material due to the large wavelength range relevant for passive cooling materials. The availability of precise theoretical data spanning several orders of magnitude is a limitation of our theoretical approach.

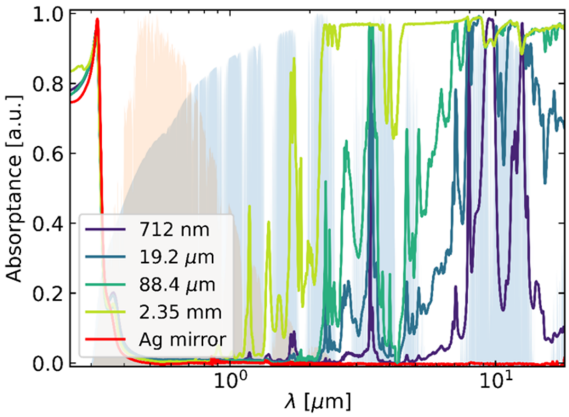

Figure 5. Absorptance of the respective PDMS samples with different thicknesses on Ag mirrors from UV–vis to mid-IR range.

3.3. Rooftop Measurements

We experimentally determined the passive cooling performance of PDMS films with different thicknesses by a rooftop experiment to verify the theoretical expectation. PDMS films were prepared on Ag-coated silicon wafers by spin coating or attachment (see Experimental Section). As shown in **Figure 6**, samples were placed individually in self-built setups for rooftop measurements.

Styrofoam insulation was applied to the outside to reduce conduction, and a low-density polyethylene (LDPE) cover was used to minimize convection, respectively. Additionally, the entire setup was covered with Al foil to reflect most of the solar irradiation. To ensure comparability between the different setups, the variety between each setup was first checked by tracking the temperature of five identical Al mirrors in daytime (Figure S6, Supporting Information). A minor deviation of ≈0.5 °C was observed during a 1.5 h rooftop measurement, under the average direct sunlight irradiation of 857 W m^{-2}.

In the daytime experiment, as an LDPE foil is applied to prevent convection, a slight greenhouse effect is apparent in the measurement cell,[17] which results in a temperature elevation of all measured samples when exposed to the sunlight. As shown in Figure 6b, the temperature of the bare Ag mirror itself increased by ≈7 °C at an average direct sunlight irradiation of 754 W m^{-2}, compared to air temperature. We attribute this greenhouse effect to a parasitic solar absorption of the sample holder and of the Ag mirror itself. Consistently, we do not observe this increase of the temperature baseline during nighttime, where the Ag mirror exhibits a similar temperature to air. To have a precise comparison and to emphasize the impact of the layer thickness on the passive cooling performance of the emitter, the measured temperature of the PDMS films with different thicknesses is, therefore, compared to the bare Ag mirror. During the experiment, the Ag mirror is exposed to comparable measurement conditions as the samples (Figure 6c,e). We, therefore, use the Ag mirror temperature as reference

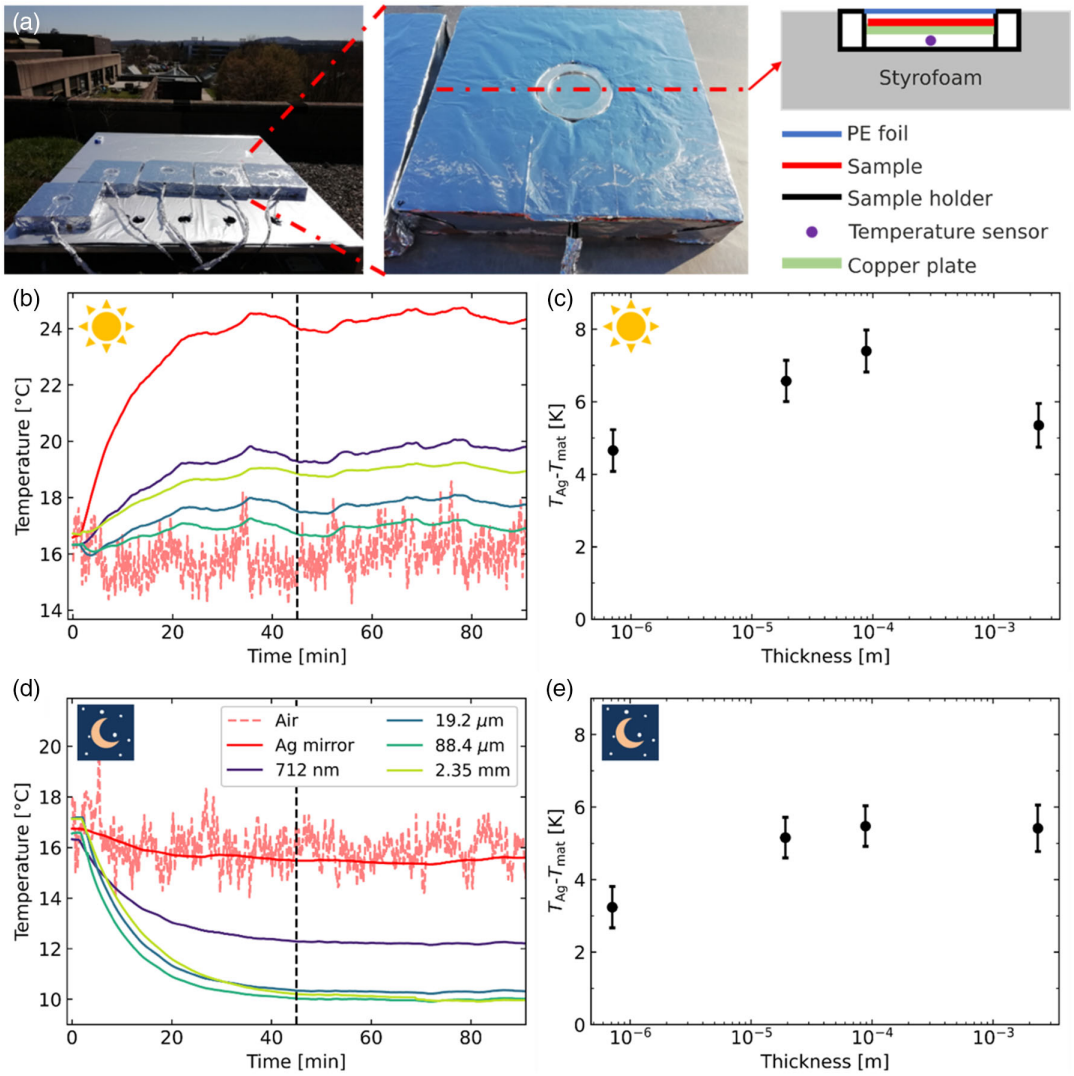

Figure 6. Rooftop measurement for PDMS films at day- and nighttime. a) Photographs and schematic of the setup for rooftop measurements. Temperature tracking of PDMS films on Ag mirror with different thicknesses, i.e., 712 nm, 19.2 μm, 88.4 μm, and 2.35 mm, and the bare Ag mirror, b) daytime and d) nighttime. The average solar irradiation during the entire daytime measurement was 754 W m^{-2}. The temperature difference between the bare Ag mirror and the PDMS films as a function of layer thickness at c) daytime and e) nighttime, respectively. The measurement was carried out under a clear sky on 23.04.2021, Bayreuth, Germany.

instead of the air temperature, which is susceptible to measurement conditions, e.g., location or wind speed.

In the nighttime experiment (Figure 6d), the passive cooling effect of the PDMS films is directly observable. All films cool down from their initial temperature (air temperature) after exposure to the clear sky until a steady state was approached. By contrast, the Ag mirror reference exhibited only an insignificant temperature reduction, which is likely attributed to the thin passivating layer of SiO_2.

To compare the cooling performance of the samples, we extracted the steady-state temperature difference between PDMS films and the Ag mirror reference from the experiments. The average temperature difference data in the steady state regime (after 45 min) are displayed in Figure 6c,e. During daytime, the temperature difference increased from 4.7 K for the 712 nm thick film to 7.4 K for the 88.4 μm film. We attribute this increase in passive cooling performance to the increased overall emittance of the film. In contrast, the passive cooling performance is reduced for the much thicker 2.35 mm PDMS film. In this case, the temperature difference dropped to 5.3 K. We attribute this drop to the increased absorption of solar radiation, as discussed in Section 4.1 (Figure 3a). For the nighttime case, the observed temperature difference between films and reference increases with increasing film thickness, reaching a plateau at high thicknesses. For the larger thicknesses, the temperature difference is not significantly increased further.

Despite the differences in the assumptions made in the calculations and actual experimental conditions, the observations of thickness-dependent passive cooling performance of PDMS films are in good agreement with the results obtained from

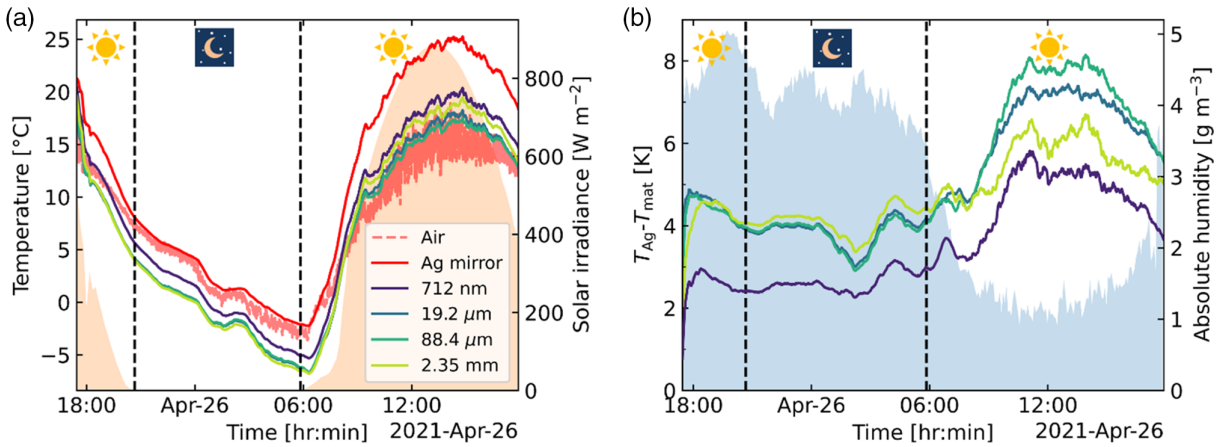

Figure 7. 24 h rooftop measurement of PDMS films with different thicknesses. a) Temperature tracking of different samples. Corresponding solar irradiation is plotted as the background. b) Temperature difference between Ag mirror and the PDMS films ($T_{Ag} - T_{mat}$) during the entire measurement, along with the absolute humidity (AH). The measurement was carried out under a clear sky, on 25–26.04.2021, Bayreuth, Germany.

our theoretical calculations. Sources of error having the most significant influence are deviations of the actual solar and atmospheric spectra to the ones used for calculation, as well as deviations of the sample's optical properties from those calculated by the optical constants. Also, the exact determination of the comprehensive heat transfer coefficient would increase the accuracy of the calculations but is a nontrivial task. As many parameters influence the net cooling power in complex and entangled dependencies, the agreement of theory and experiment is nevertheless very convincing. All the mentioned sources of error affect the absolute values of the equilibrium temperature, but not the day- and nighttime dependence trend.

To ensure that the observed behavior of the samples with different thicknesses is also valid for a more extended measurement time, we performed continuous measurements (from 18:00, 25th to 18:00, 26th April 2021, University of Bayreuth, Bayreuth, Germany). The measured temperatures of the different samples and an Ag reference are presented in **Figure 7**a. All PDMS films with different thicknesses exhibit a lower temperature than the Ag mirror in the entire 24 h measurement. The overall temperatures are lower during nighttime and increase with the onset of solar irradiance. To further reveal the thickness dependence on the cooling performance of PDMS films, the temperature difference ($T_{Ag} - T_{mat}$) is plotted in Figure 7b. A maximum temperature difference of 3.2, 4.4, 4.3, and 4.7 K was obtained for the 712 nm, 19.2 μm, 88.4 μm, and 2.35 mm PDMS films during nighttime, respectively. In contrast, a maximum temperature difference of 5.8, 7.4, 8.1, and 6.7 K was observed from the 712 nm, 19.2 μm, 88.4 μm, and 2.35 mm PDMS films in daytime. The observed temperature difference is consistent with our previous observations in short-time rooftop measurements and the simulation result. Again, for the nighttime case, except for the thinnest sample, the different thicknesses reach similar temperature differences in accordance with the short-time measurement. During daytime, the different thicknesses spread out, revealing the optimum thickness effect.

The absolute temperature difference is smaller for the nighttime period of the experiment compared to the daytime. This observation is counterintuitive because, during daytime, additional cooling power is lost by the absorption of solar radiation. However, the absolute sample temperature is lower at nighttime, so a reduced cooling power is apparent. Besides the absolute temperature also the humidity in the atmosphere is affecting the cooling potential. We monitored the relative humidity (RH) next to the experimental setup and calculated the AH present to account for changes in temperature (Figure 7b). The atmosphere's higher water content during nighttime decreases the atmospheric transparency, and hence the atmospheric radiance increases, leading to a smaller equilibrium temperature difference.

4. Conclusion

In this work, we presented a complex refractive index-based method to determine the optimum thickness for passive-cooling emitter materials in a back-reflector configuration. We observed optimum thicknesses in both day- and nighttime applications, depending on the optical properties of the material. The optimum thickness significantly influences the daytime application, while it is rather a factor in minimizing fabrication costs at maximum cooling capacity during nighttime. Our calculations further confirmed that a cooler with the highest ambient temperature cooling power does not necessarily reach the lowest equilibrium temperature. Our approach focuses on materials that use a back-reflector geometry to prevent solar heat uptake. The theoretical prediction can also be used for coolers that operate with a solar filter layer or rely on a scattering approach. For these calculations, the model needs to be adjusted to deal with the solar radiation term properly. Especially, proper complex refractive index characterization and theoretical description of a highly scattering material can be challenging. Overall, we emphasize that in addition to the passive cooling material and its nano/microstructure, the layer thicknesses of the passive cooling device needs to be optimized as well.

5. Experimental Section

Calculations: An atmospheric temperature of 298.15 K was used for both day- and nighttime to calculate the cooling power. All integrations were done using the trapezoidal integration method in Matlab. As functions inside the integrals need to have the same energy spacing to perform numerical integration, the spectral radiative powers of the sun and atmosphere are adapted to the complex refractive index spacing of the material because they are available in higher resolution. This adaption was done using the 1D data interpolation method in Matlab.

Fabrication of PDMS Films on Ag Mirrors: PDMS films with different thicknesses were prepared on protected silver mirrors. For the mirrors, a 100 nm-thick Ag layer was thermally evaporated on the wafer. Following, a 10 nm-thick layer of silicon oxide was deposited with a sputter coating step. This additional protection layer is used to prevent oxidation of the silver layer after PDMS deposition. A prepolymer mixture of PDMS (Sylgard 184, Dow Chemical) with a mixing ratio of prepolymer to cross-linker of 10:1 (by mass) was degassed in a desiccator with reduced pressure. The mixture was spin-coated on the mirrors with 1000 and 3000 rpm to obtain layers with ≈100 and 20 µm thickness, respectively. For the approximately 1 µm-thick PDMS layer, the prepolymer/cross-linker mixture was diluted to a 25 wt% solution with *n*-hexane. The mixture was then spin-coated onto the silver mirror with 4000 rpm. The layers were cured at room temperature over 48 h. For the sample with 2.35 mm thickness, the prepolymer mixture was filled in a mold and cured at 75 °C for 1.5 h. A circular piece with a diameter of approximately 5 cm was cut and gently placed on a silver mirror.

The sample thickness of the thinner samples (712 nm, 19.2 µm, and 88.4 µm) was determined with a 3D laser scanning microscope (LEXT OLS 5000, Olympus). A small incision was made to determine the actual height of the polymer layer. An area of 258 μm^2 around the incisions was imaged, and the height difference was determined by averaging the two major height fractions present in the image. The 2.35 mm high sample height was determined with a touch probe (Litematic VL-50, Mitutoyo). Different spots on the sample were measured, and the resulting height values were averaged.

Optical Characterization with UV–vis and FTIR Spectroscopy: UV–vis reflectance *R* was measured with a UV–vis spectrometer (Cary 5000, Agilent Technologies) equipped with an integrating sphere accessory (Labspheres). The measurements were conducted at the reflection port of the sphere with a fixed incident angle of 8°. As a reference, a Spectralon diffuse reflectance standard (Labspheres) was used. The FTIR spectroscopy measurements were conducted with an IR spectrometer (Vertex 70, Bruker) combined with a gold-coated integrating sphere accessory (A562, Bruker). The measurements were performed at the lower reflection port of the accessory (non-normal incidence). As a reference, a gold mirror was used. The absorptance (emittance) *A* was calculated considering the energy conservation with $A = 1–R$ assuming that transmission can be neglected due to the silver layer.

Rooftop Performance Experiment: All rooftop measurements were carried out on the roof of a four-floor building (University of Bayreuth, Bayreuth, Germany) under a clear sky. The emitter was placed in a homemade sample holder (3D printed with material of acrylonitrile butadiene styrene), which was thermally insulated by Styrofoam and covered with Mylar aluminum Foil (Figure 6a). LDPE foil with a thickness of ≈10 µm was applied to the sample holder to prevent convection. The emitter temperatures were measured by PT100 temperature sensors and recorded by a digital multimeter (DAQ6510, Tektronix, Germany) every 5 s. Air temperature is measured with a thermal couple (T-type) which is placed in the ambient environment next to the setup. The solar irradiance data are obtained from the weather station University Bayreuth (Ecological-Botanical Garden, 400 m away from the rooftop measurement). During the rooftop measurement, all sample setups were first stored under the table to achieve a similar starting temperature. A few minutes after the start of data recording, the sample setups were placed on the table to face the sky. Short- and long-term measurements were conducted for 1.5 and 24 h, respectively. During the measurements, the RH was tracked with a temperature logger (LOG220, DOSTMANN electronic GmbH) next to the setup. The AH in $g\,m^{-3}$ was calculated using RH in percent and the ambient temperature T_{amb} in °C by $AH = \frac{6.112 \cdot \exp\left(\frac{17.67 \cdot T_{amb}}{T_{amb}+243.5}\right) \cdot RH \cdot 2.1674}{273.15 + T_{amb}}$.

Supporting Information

Supporting Information is available from the Wiley Online Library or from the author.

Acknowledgements

K.H. and T.L. contributed equally to this work. The authors gratefully acknowledge the contributions of M.Sc. Thomas Tran, Stefan Rettinger for technical support and Klaus Müller for the metal evaporation. The solar radiance data were kindly provided by Prof. Christoph Thomas. This project has received funding from the European Research Council (ERC) under the European Union's Horizon 2020 research and innovation program (grant agreement no. 714968).

Conflict of Interest

The authors declare no conflict of interest.

Data Availability Statement

Research data are not shared.

Keywords

complex refractive index, radiative cooling, radiative heat transfer, thermal emission, thermal management

Received: October 6, 2021
Revised: October 30, 2021
Published online: November 16, 2021

[1] a) M. M. Hossain, M. Gu, *Adv. Sci.* **2016**, *3*, 1500360; b) B. Zhao, M. K. Hu, X. Z. Ao, N. Chen, G. Pei, *Appl. Energy* **2019**, *236*, 489.
[2] a) A. P. Raman, M. A. Anoma, L. Zhu, E. Rephaeli, S. Fan, *Nature* **2014**, *515*, 540; b) N. W. Pech-May, T. Lauster, M. Retsch, *ACS Appl. Mater. Interfaces* **2021**, *13*, 1921.
[3] a) J. Mandal, Y. Fu, A. C. Overvig, M. Jia, K. Sun, N. N. Shi, H. Zhou, X. Xiao, N. Yu, Y. Yang, *Science* **2018**, *362*, 315; b) T. Wang, Y. Wu, L. Shi, X. Hu, M. Chen, L. Wu, *Nat. Commun.* **2021**, *12*, 365.
[4] a) A. R. Gentle, G. B. Smith, *Nano Lett.* **2010**, *10*, 373; b) Y. Zhai, Y. Ma, S. N. David, D. Zhao, R. Lou, G. Tan, R. Yang, X. Yin, *Science* **2017**, *355*, 1062.
[5] a) J. L. Kou, Z. Jurado, Z. Chen, S. H. Fan, A. J. Minnich, *ACS Photonics* **2017**, *4*, 626; b) Y. Zhou, H. M. Song, J. W. Liang, M. Singer, M. Zhou, E. Stegenburgs, N. Zhang, C. Xu, T. Ng, Z. F. Yu, B. Ooi, Q. Q. Gan, *Nat. Sustain.* **2019**, *2*, 718; c) U. Banik, A. Agrawal0, H. Meddeb, O. Sergeev, N. Reininghaus, M. Gotz-Kohler, K. Gehrke, J. Stuhrenberg, M. Vehse, M. Sznajder, C. Agert, *ACS Appl. Mater. Interfaces* **2021**, *13*, 24130.
[6] a) E. Torgerson, J. Hellhake, *Sol. Energy Mater. Sol. Cells* **2020**, *206*, 110319; b) N. W. Pech-May, M. Retsch, *Nanoscale Adv.* **2020**, *2*, 249.
[7] a) W. L. Huang, Y. J. Chen, Y. Luo, J. Mandal, W. X. Li, M. J. Chen, C. C. Tsai, Z. Q. Shan, N. F. Yu, Y. Yang, *Adv. Funct. Mater.* **2021**, *31*,

2010334; b) H. Kim, S. McSherry, B. Brown, A. Lenert, *ACS Appl. Mater. Interfaces* **2020**, *12*, 43553.
[8] Y. L. Li, L. Z. Li, L. Guo, B. W. An, *Opt. Mater. Express* **2020**, *10*, 1767.
[9] a) Y. Tian, L. Qian, X. Liu, A. Ghanekar, G. Xiao, Y. Zheng, *Sci. Rep.* **2019**, *9*, 19317; b) Y. Q. Zhu, Y. H. Ye, D. Wang, Y. R. Cao, *OSA Continuum* **2021**, *4*, 416.
[10] R. Zhu, D. Hu, Z. Chen, X. Xu, Y. Zou, L. Wang, Y. Gu, *Nano Lett.* **2020**, *20*, 6974.
[11] a) H. H. Kim, E. Im, S. Lee, *Langmuir* **2020**, *36*, 6589; b) C. Sheng, Y. An, J. Du, X. Li, *ACS Photonics* **2019**, *6*, 2545; c) L. Zhu, A. P. Raman, S. Fan, *Appl. Phys. Lett.* **2013**, *103*, 223902; d) Y. Chen, J. Mandal, W. Li, A. Smith-Washington, C. C. Tsai, W. Huang, S. Shrestha, N. Yu, R. P. S. Han, A. Cao, Y. Yang, *Sci. Adv.* **2020**, *6*, eaaz5413; e) G. J. Lee, Y. J. Kim, H. M. Kim, Y. J. Yoo, Y. M. Song, *Adv. Opt. Mater.* **2018**, *6*, 1800707.
[12] R. A. Yalçın, E. Blandre, K. Joulain, J. Drévillon, *ACS Photonics* **2020**, *7*, 1312.
[13] a) B. J. Park, J. P. Pantina, E. M. Furst, M. Oettel, S. Reynaert, J. Vermant, *Langmuir* **2008**, *24*, 1686; b) A. Berk, P. Conforti, R. Kennett, T. Perkins, F. Hawes, J. v. d. Bosch, in *6th Workshop on Hyperspectral Image and Signal Processing: Evolution in Remote Sensing (WHISPERS)*, IEEE, Lausannne, Switzerland **2014**, p. 1.
[14] B. Bhatia, A. Leroy, Y. Shen, L. Zhao, M. Gianello, D. Li, T. Gu, J. Hu, M. Soljacic, E. N. Wang, *Nat. Commun.* **2018**, *9*, 5001.
[15] C. G. Granqvist, A. Hjortsberg, *J. Appl. Phys.* **1981**, *52*, 4205.
[16] a) X. Zhang, J. Qiu, X. Li, J. Zhao, L. Liu, *Appl. Opt.* **2020**, *59*, 2337;
b) X. Zhang, J. Qiu, J. Zhao, X. Li, L. Liu, *J. Quant. Spectrosc. Radiat. Transfer* **2020**, *252*, 107063; c) M. Querry, *in US Army Rep. CRDECCR-88009*, **1987**.
[17] a) S. Y. Jeong, C. Y. Tso, J. Ha, Y. M. Wong, C. Y. H. Chao, B. Huang, H. Qiu, *Renewable Energy* **2020**, *146*, 44; b) D. Chae, M. Kim, P. H. Jung, S. Son, J. Seo, Y. Liu, B. J. Lee, H. Lee, *ACS Appl. Mater. Interfaces* **2020**, *12*, 8073.